

Resonant Raman scattering in ion-beam-synthesized Mg₂Si in a silicon matrix

M. Baleva*

Faculty of Physics, Sofia University, 5 J. Boucher Boulevard, 1164 Sofia, Bulgaria

G. Zlateva

Department of Physics and Biophysics, Medical University, 2 Zdrave Strasse, 1431 Sofia, Bulgaria

A. Atanassov and M. Abrashev

Faculty of Physics, Sofia University, 5 J. Boucher Boulevard, 1164 Sofia, Bulgaria

E. Goranova

Central Laboratory for Solar Energy and New Energy Sources, BAS, 72 Tzarigradsko Chaussee Boulevard, Sofia 1784, Bulgaria

(Received 6 April 2005; published 22 September 2005)

Resonant Raman scattering by ion beam synthesized in silicon matrix Mg₂Si phase is studied. The samples are prepared with the implantation of ²⁴Mg⁺ ions with dose 4×10^{17} cm⁻² and with two different energies 40 and 60 keV into (100)Si substrates. The far infrared spectra are used as criteria for the formation of the Mg₂Si phase. The Raman spectra are excited with different lines of Ar⁺ laser, with energies of the lines lying in the interval from 2.40 to 2.75 eV. The resonant scattering can be investigated using these laser lines, as far as according to the Mg₂Si band structure, there are direct gaps with energies in the same region. The energy dependences of the scattered intensities in the case of the scattering by the allowed F_{2g} and the forbidden LO-type modes are experimentally obtained and theoretically interpreted. On the base of the investigation energies of the interband transitions in the Mg₂Si are determined. It is found also that the resonant Raman scattering appears to be a powerful tool for characterization of a material with inclusions in it. In the particular case it is concluded that the Mg₂Si phase is present in the form of a surface layer in the sample, prepared with implantation energy 40 keV and as low-dimensional precipitates, embedded in the silicon matrix, in the sample, prepared with the higher implantation energy.

DOI: [10.1103/PhysRevB.72.115330](https://doi.org/10.1103/PhysRevB.72.115330)

PACS number(s): 78.30.-j, 61.72.Ww, 61.82.Fk

I. INTRODUCTION

In recent years there has been continuously increasing interest in a new class of semiconducting materials—the transition metal silicides. Metal silicides have been widely used in silicon device technology for many years. Most of them exhibit good metallic properties suitable for use as gate electrodes and interconnections. The compound Mg₂Si is among the few semiconducting silicides. The semiconducting silicides are compatible with the well-developed silicon technology and provide new prospects for silicon-based integration. Possible applications are in thermoelectricity, photovoltaics, and optoelectronics. On the other hand, due to the large abundance and nontoxicity, the semiconducting silicides have attracted much interest as environment friendly materials.

The Mg₂Si is the one of the scarcely studied among semiconducting silicides mainly due to the difficulties in the growth of the material. The Mg₂Si is the only silicide in the system Mg-Si and according to the Mg-Si phase diagram¹ it melts congruently at 1085 °C. Nevertheless, during the growth from melt one has to take care about the considerable evaporation of the Mg component as far as the boiling point of the pure Mg is very close to the compound melting temperature.

The phonon modes dispersion curves of Mg₂Si have been calculated by several authors.^{2–6} The compound is a cubic semiconductor that crystallizes in the antifluorite structure

with one molecular unit per primitive cell and four formulas per fcc unit cell, space group $Fm\bar{3}m$. With three atoms per unit cell, group theory predicts six optical branches in the vibrational dispersion curves, which degenerate into two triply degenerate points in the center of the Brillouin zone, at wave vector $\vec{q}=0$. The symmetries of these two points are described by F_{2g} and F_{1u} irreducible representations of the group and correspond to the zone-centered Raman-active and infrared-active phonons, respectively. Because of the macroscopic electric field, associated with the F_{1u} mode, there is a TO-LO splitting at $\vec{q}=0$ for this phonon, with corresponding frequencies ω_{TO} and ω_{LO} , related through the well-known Lyddane-Sachs-Teller (LST) relation $(\omega_{LO}/\omega_{TO})^2 = \epsilon_0/\epsilon_\infty$, where ϵ_0 and ϵ_∞ are low- and high-frequency dielectric constants of the material, respectively.

The experimental studies of the Raman scattering on bulk samples show that the compound exhibits resonant scattering for light excitation energies in the range from 2.00 to 2.80 eV.^{7–9} An exciting aspect of the Raman scattering in the material is the resonance-induced scattering by the normally Raman-inactive LO-type modes.⁸ The band structure of Mg₂Si is also calculated^{10,11} and compared with the experimental results, obtained from reflectance¹² and electroreflectance¹³ measurements. It is very well established that the material exhibits strong absorption in the range between 2.0 and 3.0 eV. According to Scouler *et al.*,¹² the leading peak in the reflectivity spectrum in the above energy range is at 2.7 eV.

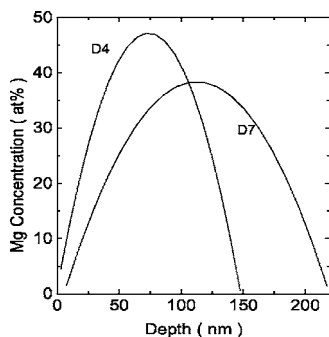


FIG. 1. Mg implantation profiles at two different energies, 40 keV (D4) and 60 keV (D7). The profiles are simulated by SRIM.

The experimental investigations of the optical properties of Mg_2Si thin films are scarcer. Due to the low condensation coefficient and high vapor pressure of Mg, the thin films formation appears to be difficult. The very low condensation coefficient of Mg as well as the limited Mg_2Si films thickness, due to the barrier behavior of Mg_2Si ,¹⁴ can be overcome using the ion-beam synthesis (IBS) method.¹⁵

The purpose of the work is to study the resonant Raman spectra of samples, representing silicon matrix with Mg_2Si embedded in it, to determine the energies of the interband transitions, inducing a resonant Raman scattering, and to compare the results with those obtained on bulk samples. The samples under investigation are prepared at different technological conditions. The interpretation of the Raman spectra and the intensity dependences on the laser excitation also gives information about the influence of the technological parameters on the samples structure.

II. SAMPLES PREPARATION

The samples are prepared by IBS, followed by rapid thermal annealing (RTA). The implantation of $^{24}\text{Mg}^+$ ions is performed by ion accelerator type ILU-4, allowing a high current density. As an ion plasma source pure Mg (purity 99.99), heated at 500 °C, is used. The mass separated $^{24}\text{Mg}^+$ ions with dose $4 \times 10^{17} \text{ cm}^{-2}$ are implanted with two different energies, 40 keV into *n*-type (100)Si substrates with $\rho = 4.5\text{--}5 \ \Omega \text{ cm}$ and 60 keV into *p* type of (100)Si substrates with $\rho = 2.5\text{--}5 \ \Omega \text{ cm}$. In Fig. 1 the Mg implantation profiles of the samples, implanted with different energies and denoted as D4 (40 keV) and D7 (60 keV), are given. The concentration profiles are simulated by SRIM (Stopping and Range of Ions in Matter) program. It is seen that the Mg concentration is lower than the Mg_2Si stoichiometric one (66.66 at% Mg) in the whole implantation depth. The higher implantation energy leads to lower Mg concentration and higher implantation depth.

During the implantation, in order to avoid the substrate amorphization, the substrates are heated to a temperature of about 230 °C by means of the incident ion beam (current density 10–12 $\mu\text{A cm}^{-2}$). After the implantation the samples implanted with the two different energies are annealed at the same temperature—500 °C (lower than the eutectic one¹ of about 640 °C) and for different times. Sample 41 is prepared

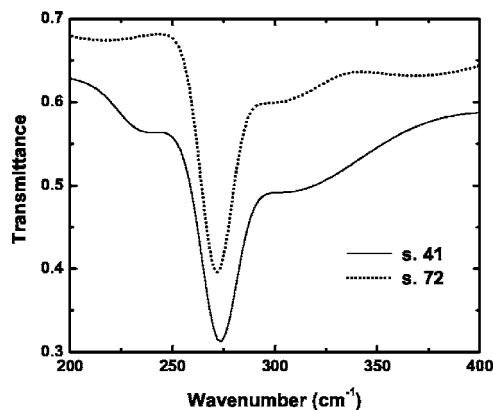


FIG. 2. IR transmittance spectra of s. 41 and s. 72, prepared at different technological conditions.

with implantation energy 40 keV (D4) and RTA for 30 s. In sample 72 the Mg ions are implanted with energy 60 keV (D7) and the duration of the RTA for this sample is 60 s.

III. EXPERIMENTAL RESULTS

A. Infrared spectra

According to the evaluations of Fenske *et al.*¹⁶ the characteristic infrared (IR) pattern should be recognized for thin films of thickness down to 10 nm, which makes the IR characterization even more sensitive in phase identification than the conventional x-ray diffraction analysis. Thus we used the IR spectra as a standard of judgment whether the Mg_2Si phase is formed in our samples. In Fig. 2 the transmittance (*T*) spectra of the samples, taken at room temperature, using the BOHMEM Fourier spectrometer, are shown in the wavenumber range from 200 to 400 cm^{-1} . A strong absorption at 272 cm^{-1} is observed in the spectra of both samples. The theoretical calculations⁶ and the experimental investigations¹⁷ give for the frequency of the one Mg_2Si IR active F_{1u} mode the values 272 and 273 cm^{-1} , respectively. The wave number position of the well-observed minima in the *T* spectra at about 272 cm^{-1} coincides fairly well with the one obtained both by theoretical calculations and experimental investigations of bulk material and can be attributed to the F_{1u} mode of the Mg_2Si phase. Thus the experimental IR spectra indicate unambiguously the formation of the Mg_2Si phase in the samples. The comparison of the spectra shows that s. 72 is more transparent than s. 41. The half-width of the absorption line in the spectrum of s. 72 (about 15 cm^{-1}), is lower than that of s. 41 (about 20 cm^{-1}). These observations can be regarded as an indication for the following: the Mg_2Si phase precipitates are much more closely distributed in s. 41, but their crystal structure is more perfect in s. 72. In other words one can think about a formation of quasicontinuous Mg_2Si layer in s. 41 and about randomly distributed precipitates in s. 72.

B. Raman-scattering spectra

The unpolarized spectra of the Raman scattering are studied at room temperature using SPEX 1403 double spectrom-

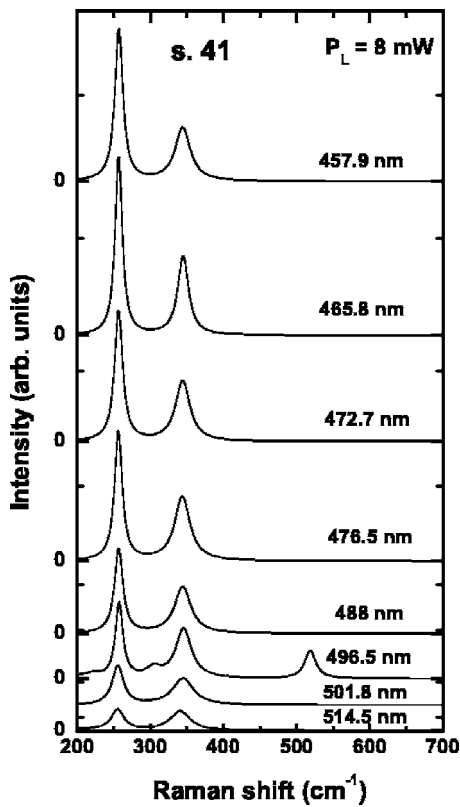


FIG. 3. The Raman spectra of s. 41, excited with eight different lines of Ar⁺ laser with power $P_L=8$ mW. The wavelengths of the laser lines are indicated.

eter, equipped with photomultiplier working in a photon counting mode. The spectra are taken with resolution 1 cm^{-1} and excited with different lines of Ar⁺ laser. The energies of the lines lay in the interval from 2.40 to 2.75 eV. According to the Mg₂Si band structure, calculated^{10,11} and experimentally proved by optical measurements,^{12,13} there are direct gaps with energies in the same region. Thus resonant scattering can be investigated by using discrete lines of Ar⁺ laser. Figures 3 and 4 show the Raman spectra of s. 41 and s. 72, excited with eight different lines. The wavelengths of the lines are listed in the figures. The spectra of s. 41 are excited with laser power $P_L=8$ mW and those of s. 72 with $P_L=24$ mW. The main structure, seen in the spectra at wave number 256 cm^{-1} , can be attributed to the first-order Raman-allowed F_{2g} phonon mode, predicted by the group theory. The theoretical calculations of Whitten *et al.*² give the value 258 cm^{-1} for the frequency of the mode. The experimental results for the F_{2g} optical phonon frequency, obtained on bulk samples and reported so far, are very similar: 258.5 cm^{-1} at 300 K according to Anastassakis and Perry,⁸ 258.3 cm^{-1} at 297 K according to Buchenauer and Cardona,⁷ and 258 cm^{-1} by Laughman and Davis¹⁸ at room temperature. A sharp peak at wave number 348 cm^{-1} is observed also in the experimental spectra, obtained by these authors. The peak is interpreted as due to the F_{1u} (LO) phonon. In our experiment a sharp peak with very close frequency is detected also, namely 345 cm^{-1} in the spectra of s. 41 and 344 cm^{-1} in the spectra of s. 72. The difference between the spectra of our samples, representing inclusions of the Mg₂Si

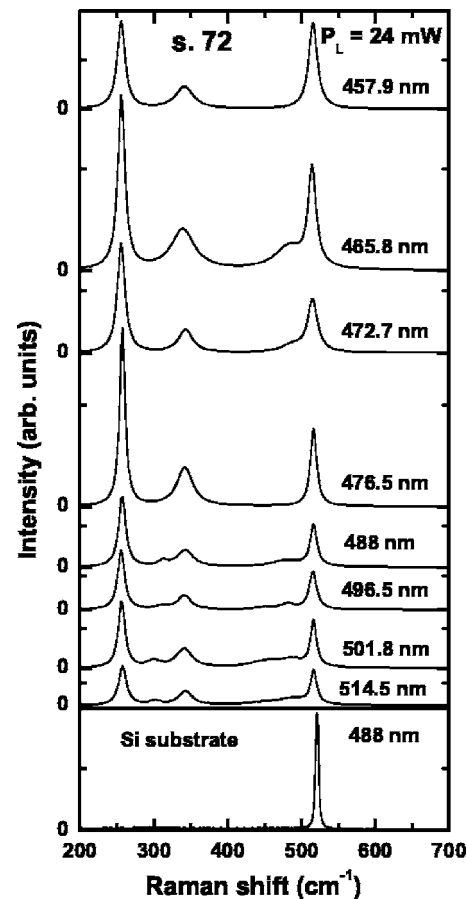


FIG. 4. The Raman spectra of s. 72, excited with eight different lines of Ar⁺ laser with power $P_L=24$ mW. The wavelengths of the laser lines are indicated. At the bottom of the figure the Raman spectrum of Si substrate is given.

phase in a silicon matrix, and those of bulk samples consists of the following: (i) a band at 696 cm^{-1} , attributed by the authors, investigating bulk samples,^{8,9} to the overtone $2LO(\Gamma)$, is not detected in our experiment and (ii) a strong line at 516 cm^{-1} , not detected in bulk samples, is seen in the spectra of s. 72 for all excitation energies and in the spectrum of s. 41, excited with $\lambda=496.5\text{ nm}$. This feature, as it follows from the phonon dispersion curves,² can be tentatively assigned to $2F_{2g}$ overtone scattering. On the other hand, the frequency of the line is very close to the one of the silicon F_{2g} Raman-active mode.

A frequency-dependent scattering intensity, as seen from Figs. 3 and 4, can be noticed for all three peaks detected. A resonant behavior of the Raman scattering in crystals is observed when the energies of the incident photons lie in the vicinity of energy gaps or critical points in the joint density of states. The measurement of the spectral dependence of the resonant-scattering amplitude yields the transition energies at the critical points. Figure 5 shows the energy dependences of the integral scattering intensities of the peak at 256 cm^{-1} for s. 41, normalized to incident light power $P_L=1$ mW and divided by ω^3 as far as the photomultiplier counts the photons number. The open squares hold for the corrected intensities, calculated from the spectra, excited with lines power 8 mW and the full squares—for those, calculated from the spectra,

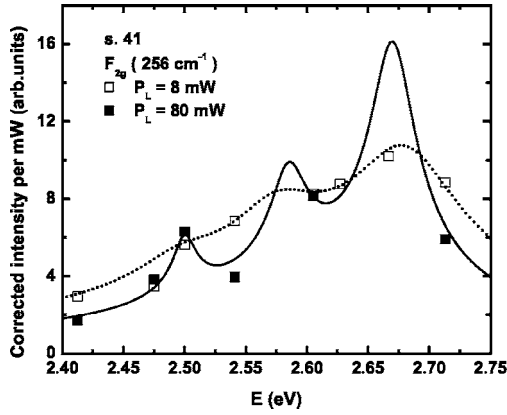


FIG. 5. The experimental energy dependences of the corrected integral intensities per mW of Raman scattering by the F_{2g} -type phonon mode in s. 41, excited with two different powers: $P_L=80$ mW (full squares); $P_L=8$ mW (open squares). The calculated curves are given with solid and dotted lines, respectively.

excited with lines power 80 mW. As far as the intensities of the different Ar^+ laser lines are quite different, a power of 80 mW is achieved only for six of the lines. The analogical dependences for the peak, which appears at 345 cm^{-1} in the spectra of s. 41, are shown in Fig. 6 with open circles and full circles, respectively. The energy dependences of the corrected integral scattering intensities, for all the three peaks, which appear in the spectra of s. 72 are displayed at Fig. 7. The open triangles represent the peak detected at 256 cm^{-1} , the open rhombs for the peak at 344 cm^{-1} , and the full triangles for the peak at 516 cm^{-1} . The corrected intensity arbitrary units, used in Figs. 5–7 are related in order to allow comparison. It is obvious from Figs. 5 and 6 that the resonant behavior is much more pronounced at a higher power of the excitation. It can be noticed also that while for s. 41 the corrected intensities of the feature at 345 cm^{-1} are higher, for s. 72 these intensities are lower.

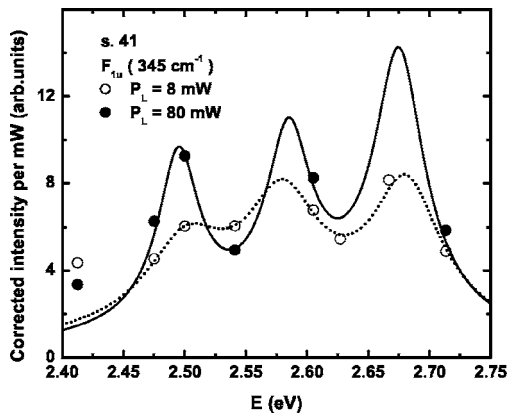


FIG. 6. The experimental energy dependences of the corrected integral intensities per mW of Raman scattering by the F_{1u} -type phonon mode in s. 41, excited with two different powers: $P_L=80$ mW (full circles); $P_L=8$ mW (open circles). The calculated curves are given with solid and dotted lines, respectively.

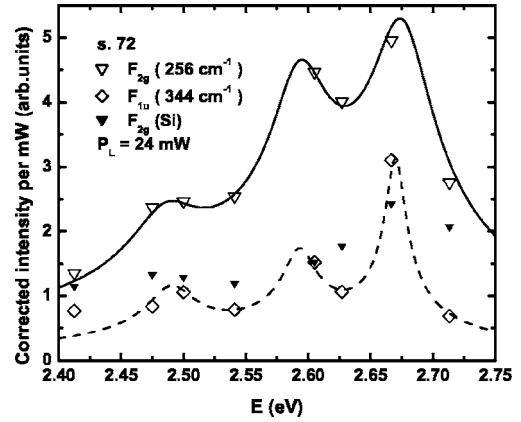


FIG. 7. The experimental energy dependences of the corrected integral intensities per mW of Raman scattering by the F_{2g} -type (open squares) and F_{1u} -type phonon modes (open rhombs) in s. 72, excited with $P_L=24$ mW. The same dependence of the scattering by the F_{2g} -type phonon of Si (full triangles) is given as well. The solid and dashed lines represent the calculated curves.

IV. DISCUSSION

A. Resonant Raman scattering by the F_{2g} -type phonon mode

Inelastic light scattering by a solid takes place with creation or annihilation of elementary excitations, usually phonons. When the phonon frequency ω_{ph} of the excitation created in the Raman process is negligible compared with the relevant electronic energies, the so-called dielectric, adiabatic, or quasistatic theory¹⁸ of the Raman tensor can be used. More exactly, the condition of the validity of the dielectric approximation is $\omega_{\text{ph}} < |\omega_L - \omega_g + i\gamma|$, where ω_L is the laser frequency, $\hbar\omega_g$ is the gap energy, and γ is the broadening parameter.

In Mg_2Si the F_{2g} phonon mode energy $\hbar\omega_{\text{ph}}=32$ meV, which is lower than the electronic states broadening and the dielectric theory is expected to apply. Theoretically, under this condition, the Raman tensor for resonant scattering around a direct gap with energy $E_g=\hbar\omega_g$ is supposed to contain terms, due to the modulation of these gaps by the phonons. These terms, called two-band terms, are proportional to the derivative of the dielectric constant and thus are strongly dispersive near E_g . The two-band model is usually used to describe the general features of the resonance by F_{2g} -type phonons. This model considers only the TO-phonon deformation potential contributions to the Raman tensor in the limit $\vec{q} \rightarrow 0$ and ignores the nonresonant terms. It applies to cubic materials and direct electron transitions. According to the model, the contribution of the two-band term to the Raman susceptibility, given by the electrical susceptibility derivative, in the approach $\omega_L \approx \omega_s$, ω_s is the scattered light frequency, and in the case of parabolic bands, is proportional to the function¹⁹

$$G(x) = x^{-2}[2 - (1-x)^{-1/2} - (1+x)^{-1/2}],$$

where $x = \omega/\omega_g$. The dispersion of the function is determined mainly by the term $(1-x)^{-1/2}$. The contribution of the remaining terms is comparable with the one of the nonresonant

TABLE I. The values of the gap energies and the broadening parameters for which a best fit of the experimental points with the calculated curves, lines in the figures, is obtained.

Sample	Phonon type	P (mW)	E_g^1 (eV)	γ_1 (eV)	E_g^2 (eV)	γ_2 (eV)	E_g^3 (eV)	γ_3 (eV)
41	TO	80	2.500	0.009	2.585	0.015	2.670	0.018
	LO	8	2.495	0.035	2.575	0.036	2.680	0.045
	TO	80	2.495	0.018	2.585	0.020	2.675	0.022
	LO	8	2.501	0.036	2.580	0.033	2.681	0.031
72	TO	24	2.485	0.027	2.593	0.023	2.675	0.025
	LO	24	2.490	0.018	2.593	0.013	2.670	0.008

terms and can be ignored. Thus in the vicinity of the resonance ($x \approx 1$) the Raman cross section is proportional to $|G(x)|^2 \propto |1-x|^{-1}$. The experimental dependences, shown in Fig. 5 with open squares and in Fig. 7 with open triangles, are interpreted as a sum of three resonance curves, given by the upper relation, for three different transition energies $E_g^i = \hbar\omega_g^i$ ($i=1,2,3$). The imaginary part $i\gamma$ is added to ω_g in order to account for the electron states broadening. The values of the gap energies and the broadening parameters for which a best fit of the experimental points with the calculated curves is obtained are summarized in Table I. The fitting is very sensitive to the change of the quantities E_g^i and accuracy of their values determination is of the order of several meV.

The later is in agreement with the consideration of the resonant Raman scattering as an even more precise method for determination of the interband transition energies than the modulation spectroscopy.¹⁹ In Table II the values of the interband transition energies, determined in this study, are

compared with the theoretical^{10,11} and experimental results^{8,9,12,13} of other authors. As it is seen, the values determined in our experiment coincide with those obtained on bulk samples by resonant Raman scattering. The assignments of the transitions, as noted by the authors^{8,9} of these studies, are only tentative. In our point of view, it is more reasonable for the leading peak in the reflectivity spectrum¹² to have the same origin as the leading peak in the resonant intensity energy dependences and the assignments of Scouler,¹² given in Table II, to be more correct.

B. Resonant Raman scattering by the forbidden one-LO-phonon mode

The forbidden resonant scattering by LO phonons consists in the change of the scattering efficiency, caused by electro-optical interaction. The LO phonons are accompanied with a longitudinal electric field, which modulates the electric susceptibility as a result of the first order electro-optical effect. Detailed calculations show that the Raman tensor in this case is proportional to the wave vector of the phonon \vec{q} and to the second derivative of the electric susceptibility. The LO scattering, being forbidden in dipole approximation ($\vec{q}=0$), will resonate more sharply than the corresponding allowed processes. In the case of forbidden resonant scattering by LO phonons two basic contributions, due to the breakdown of the selection rules and which may be activated simultaneously, are involved: (i) the wave vector mechanism which may originate either in the \vec{q} dependence of the matrix element of the Fröhlich interaction^{20,21} (intraband scattering of electrons, produced by the electric field), accompanying the longitudinal phonons, or in the wave-vector dependence of the resonant denominators²² in the vicinity of critical points and (ii) an electric field induced mechanism,^{21,23} known as

TABLE II. The experimental values of Mg₂Si interband transitions in the range from 2.00 eV to 2.80 eV, compared with the theoretical calculations (Refs. 10 and 11) and the experimental investigations of other authors; R: reflectance, ER: electroluminescence, RR: resonant scattering.

Transition and type of the critical point	E (eV); theory (Refs. 10 and 11)	E (eV); R (Ref. 11)	E (eV); ER (Ref. 12)	E (eV); RR (Refs. 8 and 9)	E (eV); this study
$M_0(\Gamma_{15}-\Gamma_1)$	2.06 ¹⁰	2.1	2.27	2.2 ⁹	
	2.20 ¹¹				
$M_0(L'_{15}-L_1)$	2.15 ¹⁰	2.2		2.60 ⁸	
				2.48 ⁹	
				2.68 ⁸	
$M_3(\Lambda_3-\Lambda_1)$	2.39 ¹⁰	2.4	2.51		2.50
				2.70 ⁹	
$M_0(X'_5-X_1)$	2.62 ¹⁰	2.6			2.59
	2.85 ¹¹				
$M_0(X'_5-X_3)$	2.74 ¹⁰	2.7			2.68
$M_0(K_4-K_1)_{45}$	2.74 ¹⁰		2.78		

Franz-Keldysh effect of resonant electric field induced scattering by LO phonons. It is pointed out²³ that the forbidden scattering in low concentration materials is attributed to \vec{q} -dependent mechanisms. The Franz-Keldysh mechanism should be important in high carrier concentration samples. In both mechanisms the leading term in the Raman tensor of the forbidden resonant scattering by LO phonons is proportional to the derivative of the corresponding term in the allowed Raman tensor or to the function $[\partial G(x)/\partial x]^2$.

In the case of superlattices²⁴ or low-dimensional structures, however, the Fröhlich interaction is not forbidden even at $\vec{q}=0$. It becomes allowed when the localization lengths of the vibrations in the sublayers or nanocrystallites are different in the conduction and valance bands. Then, as in the allowed processes, the Raman tensor of resonant scattering is proportional to the first derivative of the electric susceptibility or to the function $|G(x)|^2$.

Having taken all this into account, the analysis of our experimental results leads to the conclusion that the prevailing mechanism of scattering by LO phonons in s. 41 is a \vec{q} -dependent one. The Raman scattering by LO phonons in the sample is more intense than by the allowed one; compare Figs. 5 and 6. This means that the scattered intensity is proportional to the second derivative¹⁹ of the electric susceptibility or to the function $[\partial G(x)/\partial x]^2$. The experimental results, shown by points in Fig. 6, are interpreted as a sum of three resonance curves, proportional to this function, for the same transition energies $E_g^i = \hbar\omega_g^i$ ($i=1, 2, 3$) as in the case of the allowed resonant scattering by F_{2g} phonons. The calculated curves are given with full (80 mW) and dotted (8 mW) lines in Fig. 6. The results for the energies and the corresponding broadening parameters used to calculate the curves are included in Table I. The difference in the energies determined in both cases, allowed scattering by F_{2g} phonons and forbidden scattering by LO phonons, does not exceed 5 meV as it is seen from Table I. The broadening for the forbidden scattering as a rule is higher.

The Raman scattering by LO phonons in s. 72 is less intense than the allowed scattering by F_{2g} phonons, see Fig. 7. Then one may assume that in s. 72 the Mg_2Si phase is present in the form of low-dimensional precipitates so that the Fröhlich interaction is not forbidden even at $\vec{q}=0$ (Ref. 24) and the Raman tensor is proportional to the function $|G(x)|^2$. The curve, calculated as a sum of three terms, proportional to the function $|G(x)|^2$ with the three different values of the transition energies, is the lower curve in Fig. 7. The values of the energies and the broadening parameters, used in the calculation, are included in Table I. The difference in the energy values, obtained from the interpretation of the allowed Raman scattering by F_{2g} phonons and the allowed LO-phonon scattering does not exceed 5 meV. The broadening parameters, being proportional to the electron-phonon interaction, are lower.

The comparison of the intensity of scattering by LO phonons in s. 41 and s. 72 indicates unambiguously that the phase in s. 41 is present in the form of large grains or quasicontinuous layer, while in s.72 low-dimensional precipitates of the phase are formed in the silicon matrix. The finding is in accordance with the assumption drawn from the compar-

ison of the transmittance IR spectra of both samples. Again in accordance with the IR spectra, the broadening parameters used to interpret the scattering intensity energy dependences are in general higher for s. 41 than those for s. 72. The later implies more perfect crystal structure of the Mg_2Si phase in s. 72.

C. The line at 516 cm^{-1}

A strong line at 516 cm^{-1} , not detected in bulk samples, is seen in the spectra of s. 72 for all excitation energies and it is seen as less intensive in the spectrum of s. 41 excited with the laser line at $\lambda=496.5\text{ nm}$. It is pointed out by Anastassakis and Perry⁸ that a feature at 516 cm^{-1} , due to $2F_{2g}$ overtone scattering, as it follows from the phonon dispersion curves,² is expected to appear in the Raman scattering spectra of the Mg_2Si . The frequency-dependent Raman intensity seems to confirm this assumption. However, the feature is not observed by Anastassakis and Perry⁸ when studying the Raman scattering by bulk material. On the other hand, the peak intensity is too strong and its frequency is very close to that of the silicon F_{2g} phonon mode. The resonance of Raman scattering from the zone-center optical F_{2g} phonon in crystalline Si is studied over a wide range of energies,²⁵ including the energy of the direct transition 3.43 eV. In addition to the most prominent feature at 3.35 eV in the energy dependence of the Raman scattering, Renucci *et al.*²⁵ observe a shoulder on the main peak in the region around 2.9 eV and attribute it to indirect transitions. The behavior of the frequency-dependent scattering intensity of the peak at 516 cm^{-1} , detected in our experiment, and shown in Fig. 7 with full triangles, coincides fairly well with that reported by Renucci *et al.*²⁵ Analogically, the relatively sharp increase of the scattered intensity in our experiment starts at about 2.6 eV. The Raman spectrum of the Si substrate, taken with the laser line with wavelength 488 nm is shown at the bottom of Fig. 4. The half-width of the peak, seen in the spectrum of s. 72, is obviously larger and the peak is shifted by 4 cm^{-1} to lower frequencies. It is known²⁶ that in polycrystalline Si, due to the disorder, involved by the presence of crystallites of different sizes, the broadening may increase to 5 cm^{-1} . The broadening is asymmetric with a shoulder to lower frequencies²⁶ and possibly leads to an apparent shift of the peak. On the other hand a shift of the F_{2g} mode is usually observed when inclusions of intrinsic ions are incorporated in the silicon.²⁷

Thus the peak at 516 cm^{-1} , detected in the spectra of s. 72, can be attributed to the zone-centered F_{2g} phonons of the silicon. As far as s. 41 is concerned, a low intense and broad peak at 518 cm^{-1} is detected only in the spectrum, excited with $\lambda=496.5\text{ nm}$. This implies the conclusion that in s. 72, produced with higher implantation energy and thus with peak concentration of the implanted Mg ions much lower than the stoichiometric one, the Mg_2Si phase is present in the form of precipitates, while in s. 41 it forms surface quasicontinuous layers with a negligible quantity of randomly distributed Si.

V. CONCLUSIONS

The resonant Raman scattering appears to be a power tool for the characterization of a matrix with inclusions of a for-

eign material. The experimental investigation of the resonant scattering by samples representing silicon matrix with Mg_2Si phase leads us to the following conclusions.

(i). The detection of the matrix Raman spectrum along with the embedded phase one indicates that the phase is present in the matrix as an isolated precipitates. The silicon matrix Raman spectrum is detected in s. 72 along with the spectrum of the Mg_2Si phase. This implies that the Mg_2Si phase in the sample, prepared with an implantation of Mg^+ ions with dose $4 \times 10^{17} \text{ cm}^{-2}$ and energy 60 keV can be found in a form of precipitates. In Raman spectra of s. 41 the silicon F_{2g} phonon mode can hardly be seen. Then at the implantation of Mg^+ ions with the same dose, but with a lower energy, 40 keV, leads to the formation of closely distributed, most probably coalescent grains to form quasicontinuous surface layers.

(ii). In the particular case of Mg_2Si , where a resonant induced Raman scattering by the normally Raman-inactive LO-type modes takes place, conclusions about the sizes of the embedded precipitates can be drawn. The intensity of scattering by LO phonons in s. 41 is higher than the one of the scattering by F_{2g} -type phonon mode, indicating that the scattering by LO phonons is forbidden. The lower scattering intensity by LO phonons in comparison with the scattering by the F_{2g} -type phonon mode in s. 72 implies that the scat-

tering by LO phonons is allowed in this sample. This in its turn is an indication for the low dimension of the embedded precipitates. The broadening parameters used to interpret the scattering intensity energy dependences are in general higher for s. 41 than those for s. 72. The latter implies more perfect crystal structure of the Mg_2Si phase in s. 72.

The resonant Raman scattering appears also to be the most precise method for determination of the interband transition energies. On the base of the interpretation of the energy dependences of the Raman scattering intensities both in the case of scattering by F_{2g} -type and LO-type phonon modes we have determined energies of interband transitions in the compound Mg_2Si . In this way we contribute to the investigation of the one of the scarcely studied among the semiconducting silicides, known as "third generation semiconducting materials."

ACKNOWLEDGMENTS

The authors are indebted to B. Amov for the performing the ion-beam implantation and to G. Beshkov for the rapid thermal annealing. The work is supported by the National Fund for Scientific Investigations under Contract No. $\Phi 1301/03$ and by the Sofia University Investigation Fund.

*Electronic address: baleva@phys.uni-sofia.bg

- ¹T. B. Massalski, H. Okamoto, P. R. Subramanian, and L. Kacprzak, *Binary Alloy Phase Diagrams*, 2nd ed. (American Society for Metals, Metals Park, OH, 1990), Vol. 1, 2.
- ²W. B. Whitten, P. L. Chung, and G. C. Danielson, *J. Phys. Chem. Solids* **26**, 49 (1965).
- ³P. L. Chung, W. B. Whitten, and G. C. Danielson, *J. Phys. Chem. Solids* **26**, 1753 (1965).
- ⁴L. S. Davis, W. B. Whitten, and G. C. Danielson, *J. Phys. Chem. Solids* **28**, 439 (1967).
- ⁵R. J. Kearney, T. G. Worlton, and R. E. Schmunk, *J. Phys. Chem. Solids* **31**, 1018 (1970).
- ⁶P. H. Baranek and J. Schamps, *J. Phys. Chem. B* **101**, 9147 (1997).
- ⁷C. J. Buchenauer and M. Cardona, *Phys. Rev. B* **3**, 2504 (1971).
- ⁸E. Anastassakis and C. H. Perry, *Phys. Rev. B* **4**, 1251 (1971).
- ⁹S. Onari and M. Cardona, *Phys. Rev. B* **14**, 3520 (1976).
- ¹⁰M. Y. Au-Yang and M. L. Cohen, *Phys. Rev.* **178**, 1358 (1969).
- ¹¹B. Arnaud and M. Alouani, *Phys. Rev. B* **64**, 033202 (2001).
- ¹²W. J. Scouler, *Phys. Rev.* **178**, 1353 (1969).
- ¹³F. Vasquez, R. A. Forman, and M. Cardona, *Phys. Rev.* **176**, 905 (1968).
- ¹⁴N. Galkin, S. Vivanova, A. Konchenko, A. Maslov, and V. Pol'yarnyi (unpublished).

- ¹⁵E. Goranova, B. Amov, M. Baleva, E. P. Trifonova, and P. Yordanov, *J. Mater. Sci.* **39**, 1857 (2004).
- ¹⁶F. Fenske, H. Lange, G. Oertel, G. Reinsperger, J. Scumann, and B. Selle, *Mater. Chem. Phys.* **43**, 238 (1996).
- ¹⁷D. McWilliams and D. W. Lynch, *Phys. Rev.* **130**, 2248 (1963).
- ¹⁸L. Laughman and L. W. Davis, *Solid State Commun.* **9**, 497 (1971).
- ¹⁹M. Cardona, *Light Scattering in Solids II* (Springer, Berlin, 1982).
- ²⁰R. M. Martin, *Phys. Rev. B* **4**, 3676 (1971).
- ²¹J. G. Cay, *1971 International Conference on Light Scattering in Solids*, Paris, 1971 (Flammarion, Paris, 1971).
- ²²D. C. Hamilton, *Phys. Rev.* **188**, 1221 (1969).
- ²³A. Pinczuk and E. Burnstein, *10th International Conference on the Physics of Semiconductors*, Washington D.C., 1970 (U.S. Atomic Energy Commission, Washington, D.C., 1970).
- ²⁴P. Manuel, G. A. Sai-Halasz, L. L. Chang, Chin-An Chang, and L. Esaki, *Phys. Rev. Lett.* **37**, 1701 (1976).
- ²⁵J. B. Renucci, R. N. Tyte and M. Cardona, *Phys. Rev. B* **11**, 3885 (1975).
- ²⁶D. Bormejo and M. Cardona, *J. Non-Cryst. Solids* **32**, 421 (1979).
- ²⁷G. Lucovsky, *Solid State Commun.* **29**, 571 (1979).